Nanoscale

PAPER

View Article Online
View Journal | View Issue

Cite this: *Nanoscale*, 2017, **9**, 19124

Damage-free and rapid transfer of CVD-grown two-dimensional transition metal dichalcogenides by dissolving sacrificial water-soluble layers†

Lili Zhang,[a] Chenyu Wang,[a] Xue-Lu Liu,[b,c] Tao Xu,[d] Mingsheng Long,[a] Erfu Liu,[a] Chen Pan,[a] Guangxu Su,[a] Junwen Zeng,[a] Yajun Fu,[a] Yiping Wang,[a] Zhendong Yan,[a] Anyuan Gao,[a] Kang Xu,[a] Ping-Heng Tan,[b,c] Litao Sun,[d] Zhenlin Wang,[a] Xinyi Cui*[e] and Feng Miao*[a]

Received 17th September 2017,
Accepted 13th November 2017

DOI: 10.1039/c7nr06928f

rsc.li/nanoscale

As one of the most important family members of two-dimensional (2D) materials, the growth and damage-free transfer of transition metal dichalcogenides (TMDs) play crucial roles in their future applications. Here, we report a damage-free and highly efficient approach to transfer single and few-layer 2D TMDs to arbitrary substrates by dissolving a sacrificial water-soluble layer, which is formed underneath 2D TMD flakes simultaneously during the growth process. It is demonstrated, for monolayer MoS_2, that no quality degradation is found after the transfer by performing transmission electron microscopy, Raman spectroscopy, photoluminescence and electrical transport studies. The field effect mobility of the post-transfer MoS_2 flakes was found to be improved by 2–3 orders compared with that of the as-grown ones. This approach was also demonstrated to be applicable to other TMDs, other halide salts as precursors, or other growth substrates, indicating its universality for other 2D materials. Our work may pave the way for material synthesis of future integrated electronic and optoelectronic devices based on 2D TMD materials.

Introduction

2D TMDs have emerged as promising candidates for post-silicon electronics due to their atomically thin geometry and unique electronic properties.[1–4] As a readily accessible and economical approach for industrial scale synthesis, the chemical vapor deposition (CVD) technique has achieved great success in the growth of graphene,[5,6] 2D TMDs and related heterostructures.[7–30] These samples grown on certain substrates are not readily available for device fabrication owing to strong interactions between the samples and substrates. Therefore, a damage-free and efficient transfer of as-grown 2D TMD samples to target substrates is a predominantly key prerequisite for facilitating their future applications.

So far, two main types of methods developed to transfer 2D TMDs have been focused on the treatment after sample growth. One is the chemical etching of the growth substrates using a strong acid or alkali chemical.[7,11–13,16,23,26,31,32] The other is peeling off 2D TMDs by significantly strong adhesion between 2D TMDs and supporting layers.[33–35] Recently, ultrasonication-assisted and water penetration transfer approaches were also reported,[36–42] where water molecules or bubbles penetrate into the interface between 2D TMDs and growth substrates to lift off 2D TMDs. However, due to chemical contamination and limitations in choosing appropriate adhesion layers or substrates, these processes may have issues in damage control, time efficiency and cost. Thus, a damage-free, rapid and economic strategy to overcome these challenges is highly demanded.

Here, we report a damage-free, time-efficient and cost-effective strategy to grow (CVD) and transfer 2D TMDs films to arbitrary target substrates. We choose a representative TMD material, MoS_2, and demonstrate such a strategy by growing and dissolving a sacrificial crystal layer (NaS_x and NaCl) under-

[a]National Laboratory of Solid State Microstructures, School of Physics, Collaborative Innovation Center of Advanced Microstructures, Nanjing University, Nanjing 210093, China. E-mail: miao@nju.edu.cn
[b]State Key Laboratory of Superlattices and Microstructures, Institute of Semiconductors, Chinese Academy of Sciences, Beijing 100083, China
[c]College of Materials Science and Opto-Electronic Technology, University of Chinese Academy of Sciences, Beijing 100049, China
[d]SEU-FEI Nano-Pico Center, Key Laboratory of MEMS of Ministry of Education, Southeast University, Nanjing 210096, China
[e]State Key Laboratory of Pollution Control and Resource Reuse, School of the Environment, Nanjing University, Nanjing 210046, China.
E-mail: lizzycui@nju.edu.cn

†Electronic supplementary information (ESI) available: Schematic setup for material synthesis, additional characterizations on water-soluble substance and transferred MoS_2 flakes, synthesis and transfer of $MoSe_2$ flakes, synthesis and transfer of MoS_2 flakes using different halide salts, synthesis and transfer of MoS_2 flakes on sapphire and glass substrates. See DOI: 10.1039/c7nr06928f

neath the MoS_2 flakes, which is formed spontaneously with MoS_2 *via* the sulfurization of a NaCl and MoO_3 mixture precursor. The approach is entirely different from the previously reported methods. No quality degradation was found after the transfer according to Raman and photoluminescence (PL) characterization. The whole lift-off and transfer processes could be accomplished within one minute. Field-effect transistors (FETs) made of the transferred MoS_2 flakes show that the mobility is improved by 2–3 orders when compared with that of the as-grown ones. This generic approach is also demonstrated to be applicable to other TMDs, such as $MoSe_2$.

Experimental

Growth of MoS_2 flakes

Monolayer MoS_2 flakes were synthesized in a two-temperature zone tube furnace. In a typical procedure, mixed NaCl and MoO_3 powders with a weight ratio of 9 : 1 in a quartz boat were placed in the high-temperature zone. Another quartz boat holding 100 mg pure sulfur was placed in the upwind low-temperature zone. The distance between the two quartz boats was fixed at 18 cm. The fresh SiO_2/Si substrate was faced down above the quartz boat containing the mixed NaCl/MoO_3 powders. Before the experiments, high purity (99.99%) Ar gas was passed through the tube at a flow rate of 400 standard-state cubic centimeter per minute (sccm) for 10 min to flush. The temperatures of the two boats were then gradually increased from room temperature (RT) to target temperatures (650 °C for mixed NaCl and MoO_3 powders, and 240 °C for sulfur powders) within 25 min and kept for 10 min with 200 sccm Ar flow, followed by a cooling down process (cooled down to RT within 2 hours).

Transfer of MoS_2 flakes

A thin layer of PMMA was first spin-coated onto an as-grown wafer. One edge of the MoS_2 growth area was partially scratched before the wafer was placed in a container with DI water being gradually added. The PMMA/MoS_2 layer was lifted off and floated on the water surface after the water-soluble layer was dissolved. The layer was then transferred to new SiO_2/Si or PET (polyethylene terephthalate) substrates (Video S1 and Video S2 in the ESI†). The post-transferred PMMA/MoS_2/new substrate was then dried in air, followed by the removal of PMMA in acetone.

The device fabrication and electrical measurements

The devices with two-terminal structures were fabricated on the as-grown and transferred SiO_2/Si substrates. The electrodes (5 nm Ag/50 nm Au) were patterned using a home-made shadow mask method and deposited by standard electron beam evaporation. All the devices were measured under a N_2 atmosphere at RT using an Agilent B1500A parameter analyzer.

Optical, Raman, PL and TEM characterization

Optical images were recorded in a Nikon DIGITAL SIGHT DS-Fi2 K18680 optical microscope. Raman and PL spectra were recorded using a Jobin–Yvon HR800 Raman system, equipped with a liquid-nitrogen-cooled charge-coupled device (CCD), a 100× objective lens (NA = 0.90) and several gratings. The excitation wavelength was 532 nm from a solid state laser. The resolutions of the Raman and PL system at 532 nm were 0.35 cm^{-1} and 0.2 meV per CCD pixel depedending on the grating used. TEM measurements were carried out at 200 kV.

Results and discussion

We chose NaCl and MoO_3 as precursors owing to their similar melting points (795 °C for MoO_3 and 801 °C for NaCl).[43,44] As illustrated in Fig. 1a and b, they are heated to form vapor phases of MoO_3 and NaCl clusters. By considering that the dissociation energy of a Na–O bond (266 ± 4 kcal mol^{-1}) is larger than that of a Mo–O bond (145.1 ± 4 kcal mol^{-1}),[45,46] the unsaturated oxygen atoms on the SiO_2 substrate surface prefer to form bonds with Na^+ rather than Mo^{6+}. Such a NaO_x layer could be then vulcanized by sulfur vapor to form highly water-soluble NaS_x on the SiO_2 surface. Simultaneously, MoS_2 clusters obtained *via* the sulfurization of MoO_3 clusters could nucleate and form MoS_2 flakes on the NaS_x layer. In this case, the MoS_2 flakes might be easily lifted off and transferred after dissolving the water-soluble layer in water.

In our experiments, growth substrates (SiO_2 wafers) were placed face-up above the NaCl/MoO_3 precursors inside a tube furnace for MoS_2 synthesis (ESI Fig. S1†). Triangular monolayer MoS_2 flakes with typical sizes ranging from few ten to a few hundred micrometers (ESI Fig. S2a and S2c†) were successfully synthesized *via* the sulfuration of the NaCl/MoO_3 precursors. We indeed found that the MoS_2 flakes could be easily lifted off and transferred to target substrates by dissolving the water-soluble layer in water, as expected. As illustrated in Fig. 1c–f, a PMMA thin film was first spin-coated on the as-grown wafers. The PMMA film was then partially scratched along the edge of the MoS_2 area to allow water molecules to penetrate in. After that, the PMMA covered as-grown wafer was put into water to get the PMMA/MoS_2 film lifted off. The PMMA/MoS_2 film floating on the water surface was then transferred to the desired substrates. Lastly, the PMMA layer was removed by putting the PMMA/MoS_2/new substrate structure into acetone for several minutes. Fig. 1g–j exhibit the optical images of the same MoS_2 flake at different transfer steps. No wrinkles, cracks, or polymer residues on MoS_2 flakes or new substrates were found (Fig. 1j, ESI Fig. S2b, S2d†). In addition, the whole lift-off and transfer processes can be accomplished within one minute (ESI Videos S1 and S2†).

We first performed detailed studies on the transferred monolayer MoS_2 by using transmission electron microscopy (TEM) and X-ray photoelectron spectroscopy (XPS). Selected area electron diffraction (SAED) patterns acquired from various positions of a MoS_2 flake (Fig. 2a) are shown in Fig. 2b–d,

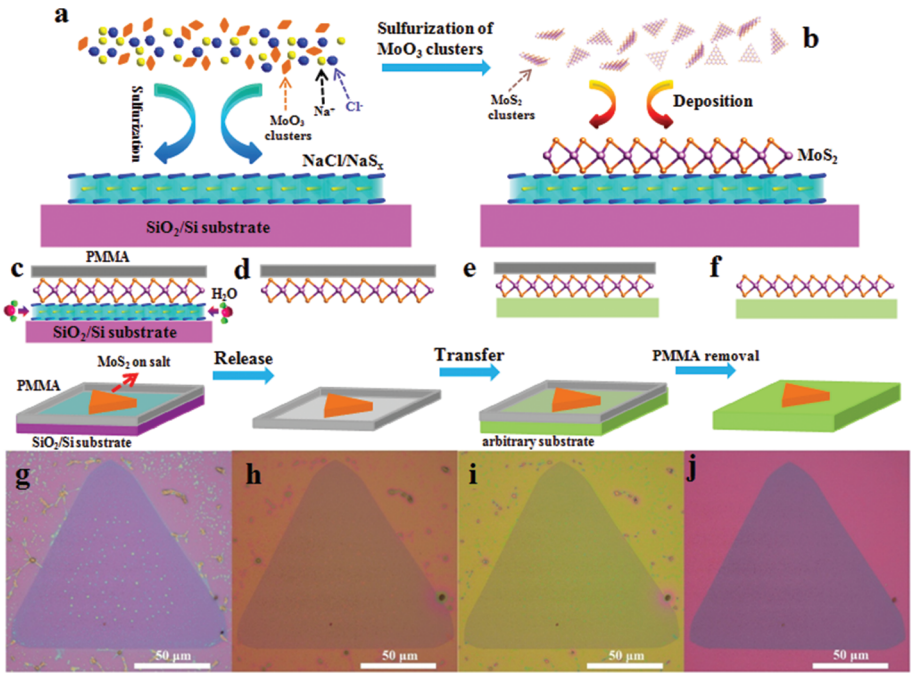

Fig. 1 Strategy design for the growth and transfer of MoS_2 flakes. (a, b) Schematic diagram of the growth of MoS_2 on a water-soluble layer. (c–f) Schematic diagrams of the release and transfer of MoS_2 in water. (g–j) Optical images of as-grown MoS_2, PMMA covered as-grown wafer, PMMA/MoS_2/new substrate and MoS_2/new substrate.

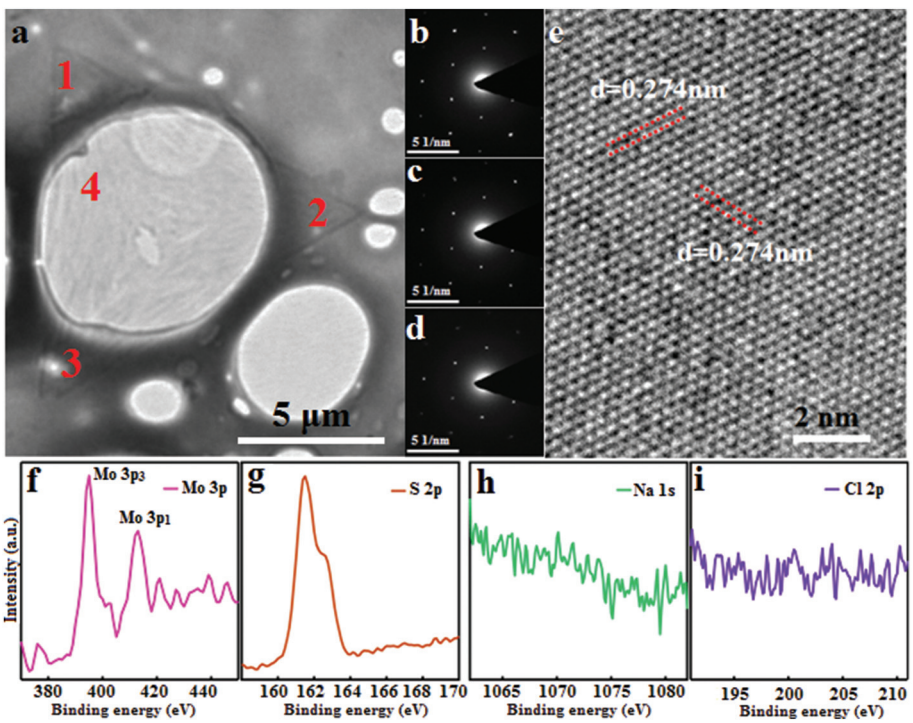

Fig. 2 TEM characterization and XPS spectra of the as-transferred MoS_2 flakes. (a) Low magnification TEM image of a monolayer MoS_2 flake supported on a holey carbon TEM grid. (b–d) SAED patterns taken at locations marked with 1 to 3 on the monolayer MoS_2 flake in (a). (e) HRTEM image of the monolayer MoS_2 flake acquired at the location marked with 4 in (a). (f–i) Mo 3p, S 2p, Na 1s and Cl 2p core-level XPS of transferred MoS_2 flakes.

which exhibit identical orientation and precise fit to the hexagonal symmetry of 2H-MoS_2. Such results demonstrate the single crystallinity of the obtained MoS_2 over a large area of tens of micrometers, indicating that our transfer processes are damage-free. As seen in Fig. 2e, the high-resolution TEM (HRTEM) image acquired at position 4 in Fig. 2a shows crystalline planes with a spacing of 0.274 nm, corresponding to the (10–10) planes of MoS_2. More importantly, no residual Na or Cl elements were detected on the transferred MoS_2 flakes based on our characterization results from XPS measurements (Fig. 2f–i, ESI Fig. S3†).

After the successful demonstration of the water-assisted transfer of MoS_2, identifying the composition of the water-soluble layer underneath the flakes is vital for understanding the growth mechanism. We scratched a MoS_2 flake partially and found a thin layer of substance underneath the MoS_2 flake as shown in Fig. 3a. A similar substance was also observed on certain parts of the growth substrate surface or beneath the edge of the MoS_2 flakes (ESI Fig. S4a†). Energy dispersive spectroscopy (EDS) analysis was carried out on this substance, with results shown in Fig. 3b and ESI Fig. S4b.† The data indicate that the major elemental compositions are Na, S and Cl, which likely originate from the NaS_x and non-vulcanized NaCl. To further confirm this, we introduced plasma irradiation to etch the MoS_2 film and characterized the water-soluble substance underneath it.[47] XPS measurement results clearly show that, after thinning MoS_2, the signals of Na and Cl elements got enhanced while that of Mo element got suppressed (ESI Fig. S5 and S6†), suggesting that Na and Cl are indeed two major elemental compositions of the water-soluble layer. More importantly, the thickness and the area of the sacrificial layer can be controlled by adjusting the experimental parameters, such as growth temperature (ESI Fig. S7 and S8†). The thickness of the sacrificial layer increased with the increasing growth temperatures from 500 °C to 800 °C (ESI Fig. S8†) and the typical thickness is ~2 nm for those synthesized at 650 °C (ESI Fig. S7c and d†). Also, we observed that the sacrificial layer is a quasi-continuous film (ESI Fig. S9†).

Since our transfer processes only involve the use of deionized water (DI water), PMMA and acetone (with no etching process involved), the approach could have advantages on keeping the pristine quality of the samples. In order to investigate it, Raman characterization was carried out on as-grown MoS_2 flakes (Fig. 4c) and the exact one after transfer (Fig. 4d) for comparison. As shown in Fig. 4a, the as-grown MoS_2 sheet exhibits two characteristic Raman bands at around 386.4 cm^{-1} and 404.5 cm^{-1}, corresponding to the E^1_{2g} (in-plane vibrations of Mo and S atoms) and A_{1g} (out-of-plane vibrations of

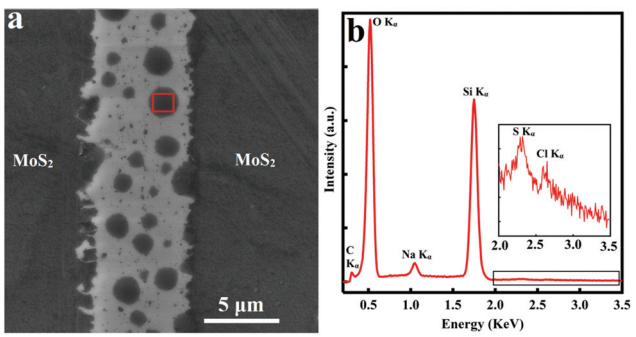

Fig. 3 EDS analysis of the water-soluble substance. (a) SEM image of the substance underneath the MoS_2 flakes. (b) EDS analysis of the substance in the red rectangle area in (a).

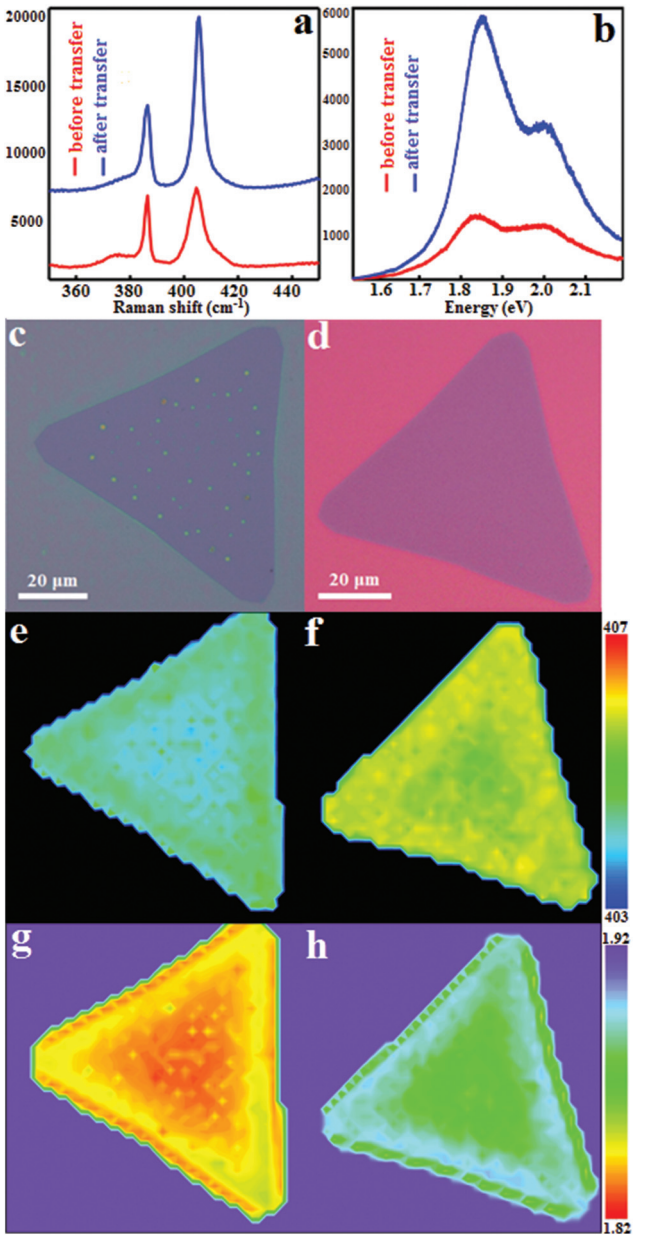

Fig. 4 Raman and PL characterization of an as-grown and transferred MoS_2 flake. (a) Raman spectra and (b) PL spectra of an as-grown and transferred MoS_2 flake. Optical images of the (c) as-grown and (d) transferred MoS_2 flake. Frequency distribution of the A_{1g} mode measured by Raman mapping for the (e) as-grown and (f) transferred MoS_2 flake. Energy distribution of A excitonic transition measured by PL mapping of the (g) as-grown and (h) transferred MoS_2 flake.

S atoms) modes of MoS_2 crystals,[48,49] respectively. The frequency difference between the two modes is about 18.1 cm^{-1}, indicating that the sample is indeed monolayer MoS_2.[48,50,51] After the transfer, while the position of the E^1_{2g} mode remains consistent, the A_{1g} mode shifts to a higher frequency located at around 405.5 cm^{-1}. We also performed the Raman mapping measurement of the A_{1g} mode before and after the transfer to examine the spatial uniformity of the grown sample. As shown in Fig. 4e, the frequency of the A_{1g} mode ranged from 403.6 to 405.5 cm^{-1} (centered at 404.5 cm^{-1}) before the transfer, which implies that the as-grown MoS_2 exhibits high crystallinity and good uniformity. In Fig. 4f, the frequency of the A_{1g} mode in a transferred MoS_2 flake is shifted to the range of 405.0 to 406.1 cm^{-1} (centered at 405.5 cm^{-1}) and it still maintains a high homogeneity. This confirms that the tranfer process is damage-free. Such a shift may arise from the reduced electron-doping level after the removal of the water-soluble layer.[48,52,53] The slightly better spatial uniformity with a narrower distribution of the A_{1g} mode observed in the sample after the transfer demonstrates quality improvement after removing the water-soluble substances during the transfer processes.

PL measurements were also performed by using the same laser excitation at room temperature, with results shown in Fig. 4b. For the as-grown flake, the strong intensity peak at around 1.85 eV (A excitonic transitions) and the relatively weak intensity peak at around 1.99 eV (B excitonic transitions) come from the direct bandgap transitions at the Brillouin zone K point.[48,54] The energy difference of 0.14 eV is ascribed to the splitting of the valence band induced by the spin–orbit coupling.[55] The intensities of both A and B exciton peaks were found to be notably enhanced after the transfer, indicating improved sample quality and luminescence quantum efficiency.[54] The energy of the A excitonic transition characterized by PL mapping (Fig. 4g and h) was observed to distribute in the ranges of 1.82–1.86 eV (centered around 1.84 eV) and 1.85–1.90 eV (centered around 1.87 eV) for the flake before and after the transfer, respectively. The PL peak at around A excitonic transition consists of two components in monolayer MoS_2, namely A exciton (neutral exciton) and A^- trion (negatively charged exciton). A^- trion appears in the MoS_2 flake with the unintentional electron doping arising from surface defects and the substrate. The component weight of A exciton and A^- trion in the PL process can be tuned *via* electrostatic or substrate-induced doping,[52,56] with more A^- trion component for heavier electron doping. Neutral excitons emit at a higher energy than charged excitons owing to the large exciton binding energy (~30 meV).[52,56] Thus, the observed overall blue-shift of the A excitonic peak after the transfer can be explained by a relative increase in the luminescence emission from neutral excitons, which implies reduced electron doping on MoS_2 after the removal of the water-soluble layer.

Since monolayer MoS_2 is a representative 2D semiconducting material, the field effect mobility is an important parameter to assess sample quality. To evaluate the electrical performance of the MoS_2 flakes, we fabricated FETs based on randomly selected 60 as-grown and 60 transferred MoS_2 flakes on SiO_2/Si substrates. Fig. 5a presents the typical transfer curves

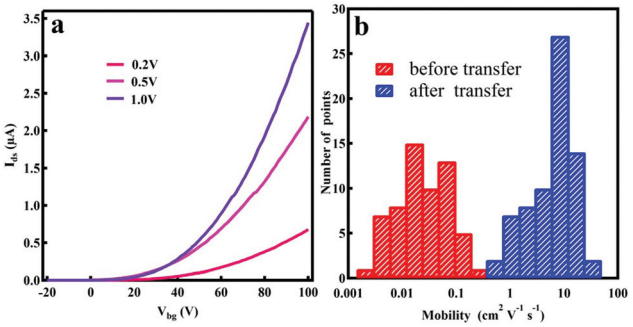

Fig. 5 Transfer curves and field effect mobility of the MoS_2 FET devices. (a) The drain–source current I_{ds} as a function of the back-gated voltage V_{bg} under different drain–source voltage V_{ds} for a transferred MoS_2 flake. (b) Statistical mobility distribution of randomly selected 60 as-grown and 60 transferred MoS_2 flakes.

of a transferred MoS_2 flake, which shows n-type conduction behavior with the on/off ratio exceeding 10^7 (ESI Fig. S10†). The field effect mobility can be extracted from the linear regime of the transfer curves using the equation $\mu = [dI_{ds}/dV_{bg}] \times [L/(WC_gV_{ds})]$, where L, W, and C_g are the channel length, width, and the gate capacitance per unit area (~1.18×10^{-8} F cm^{-2}), respectively. The statistical distribution of the field effect mobility of the as-grown and after-transfer flakes is shown in Fig. 5b. More than half of the after-transfer mobility values fall in the range of 5 to 25 cm^2 V^{-1} s^{-1}, with the highest value of 24.3 cm^2 V^{-1} s^{-1}. When compared with that of the as-grown flakes, the mobility is improved by 2–3 orders, which is likely due to the improved metal contact and reduced substrate scattering after removing the water-soluble substances.

With the realization of the growth and transfer of MoS_2, we also performed a series of systematic studies to demonstrate this approach in other 2D TMDs, by using different halide salts or different growth substrates. The results on the growth and transfer of $MoSe_2$ are shown in Section S8 in the ESI.† We found that many other halide salts can be used as precursors to grow and transfer MoS_2 flakes, including NaBr, NaI, KCl and KI (Section S9 in the ESI†). These results also indicate that halide salts play a key role in the synthesis of 2D TMDs, which has also been reported in the recent literature.[17,57–59] We also synthesized and transferred MoS_2 flakes on various substrates, such as sapphire and glass (Section S10 in ESI†). Furthermore, several literature studies have reported the successful growth of metal films, graphene and perovskite films on water-soluble NaCl and/or $Sr_3Al_2O_6$ substrates.[60–62] After dissolving these sacrificial substrates, high quality samples can be obtained. Thus, the synthesis of materials on water-soluble substrates can be used as a general way for the damage-free, rapid and inexpensive transfer of various materials in many fields.

Conclusions

In conclusion, we designed and realized a damage-free and highly efficient approach to transfer 2D TMDs to arbitrary sub-

strates by dissolving a sacrificial water-soluble layer. Such a water-soluble layer can be formed underneath TMD flakes simultaneously during the growth process. It was demonstrated, for monolayer MoS_2, that no quality degradation was found after the transfer by performing careful TEM, Raman spectroscopy, PL and electrical transport studies. This approach was also demonstrated to be applicable to other TMDs, other halide salts as precursors, or other growth substrates, indicating its universality for other 2D materials. Our work may pave the way for the material synthesis of future integrated electronic and optoelectronic devices based on 2D TMD materials.

Conflicts of interest

The authors declare no conflict of interest.

Acknowledgements

This work was supported in part by the National Key Basic Research Program of China (2015CB921600 and 2013CBA01603), National Key Research and Development Program of China (2016YFA0301204), National Natural Science Foundation of China (61574076, 11374142, 11525417, 11374137, 11374135, 11474277 and 11434010), Natural Science Foundation of Jiangsu Province (BK20140017 and BK20150055), China Postdoctoral Science Foundation, Fundamental Research Funds for the Central Universities, and Collaborative Innovation Center of Advanced Microstructures. We acknowledge Prof. Wei Ji for stimulating discussions.

References

1 D. Lembke, S. Bertolazzi and A. Kis, *Acc. Chem. Res.*, 2015, **48**, 100–110.
2 H. Schmidt, F. Giustiniano and G. Eda, *Chem. Soc. Rev.*, 2015, **44**, 7715–7736.
3 K. F. Mak and J. Shan, *Nat. Photonics*, 2016, **10**, 216–226.
4 T. Ritschel, J. Trinckauf, K. Koepernik, B. Büchner, M. V. Zimmermann, H. Berger, Y. I. Joe, P. Abbamonte and J. Geck, *Nat. Phys.*, 2015, **11**, 328–331.
5 X. Li, L. Colombo and R. S. Ruoff, *Adv. Mater.*, 2016, **28**, 6247–6252.
6 M. Li, D. Liu, D. Wei, X. Song, D. Wei and A. T. S. Wee, *Adv. Sci.*, 2016, **3**, 1600003.
7 A. L. Elías, N. Perea-López, A. Castro-Beltrán, A. Berkdemir, R. Lv, S. Feng, A. D. Long, T. Hayashi, Y. A. Kim and M. Endo, *ACS Nano*, 2013, **7**, 5235–5242.
8 T. A. Empante, Y. Zhou, V. Klee, A. E. Nguyen, I. Lu, M. D. Valentin, S. A. Naghibi Alvillar, E. Preciado, A. J. Berges and C. S. Merida, *ACS Nano*, 2017, **11**, 900–905.
9 B. Li, L. Huang, M. Zhong, N. Huo, Y. Li, S. Yang, C. Fan, J. Yang, W. Hu and Z. Wei, *ACS Nano*, 2015, **9**, 1257–1262.
10 B. Liu, M. Fathi, L. Chen, A. Abbas, Y. Ma and C. Zhou, *ACS Nano*, 2015, **9**, 6119–6127.
11 J. Shi, D. Ma, G. Han, Y. Zhang, Q. Ji, T. Gao, J. Sun, X. Song, C. Li and Y. Zhang, *ACS Nano*, 2014, **8**, 10196–10204.
12 X. Wang, Y. Gong, G. Shi, W. L. Chow, K. Keyshar, G. Ye, R. Vajtai, J. Lou, Z. Liu and E. Ringe, *ACS Nano*, 2014, **8**, 5125–5131.
13 Q. Fu, L. Yang, W. Wang, A. Han, J. Huang, P. Du, Z. Fan, J. Zhang and B. Xiang, *Adv. Mater.*, 2015, **27**, 4732–4738.
14 M. Hafeez, L. Gan, H. Li, Y. Ma and T. Zhai, *Adv. Mater.*, 2016, **28**, 8296–8301.
15 K. Keyshar, Y. Gong, G. Ye, G. Brunetto, W. Zhou, D. P. Cole, K. Hackenberg, Y. He, L. Machado and M. Kabbani, *Adv. Mater.*, 2015, **27**, 4640–4648.
16 X. Zhou, L. Gan, W. Tian, Q. Zhang, S. Jin, H. Li, Y. Bando, D. Golberg and T. Zhai, *Adv. Mater.*, 2015, **27**, 8035–8041.
17 S. Li, S. Wang, D. Tang, W. Zhao, H. Xu, L. Chu, Y. Bando, D. Golberg and G. Eda, *Appl. Mater. Today*, 2015, **1**, 60–66.
18 Y. Shi, H. Li and L. Li, *Chem. Soc. Rev.*, 2015, **44**, 2744–2756.
19 G. Su, V. G. Hadjiev, P. E. Loya, J. Zhang, S. Lei, S. Maharjan, P. Dong, P. M. Ajayan, J. Lou and H. Peng, *Nano Lett.*, 2014, **15**, 506–513.
20 K. Wu, B. Chen, S. Yang, G. Wang, W. Kong, H. Cai, T. Aoki, E. Soignard, X. Marie and A. Yano, *Nano Lett.*, 2016, **16**, 5888–5894.
21 T. Zhang, B. Jiang, Z. Xu, R. G. Mendes, Y. Xiao, L. Chen, L. Fang, T. Gemming, S. Chen, M. H. Rümmeli and L. Fu, *Nat. Commun.*, 2016, **7**, 13911.
22 Y. Lin, R. K. Ghosh, R. Addou, N. Lu, S. M. Eichfeld, H. Zhu, M. Li, X. Peng, M. J. Kim, L. Li, R. M. Wallace, S. Datta and J. A. Robinson, *Nat. Commun.*, 2015, **6**, 7311.
23 Y. Gong, J. Lin, X. Wang, G. Shi, S. Lei, Z. Lin, X. Zou, G. Ye, R. Vajtai and B. I. Yakobson, *Nat. Mater.*, 2014, **13**, 1135–1142.
24 C. Huang, S. Wu, A. M. Sanchez, J. J. Peters, R. Beanland, J. S. Ross, P. Rivera, W. Yao, D. H. Cobden and X. Xu, *Nat. Mater.*, 2014, **13**, 1096–1101.
25 X. Duan, C. Wang, J. C. Shaw, R. Cheng, Y. Chen, H. Li, X. Wu, Y. Tang, Q. Zhang and A. Pan, *Nat. Nanotechnol.*, 2014, **9**, 1024–1030.
26 M. Li, Y. Shi, C. Cheng, L. Lu, Y. Lin, H. Tang, M. Tsai, C. Chu, K. Wei and J. He, *Science*, 2015, **349**, 524–528.
27 Q. Ji, C. Li, J. Wang, J. Niu, Y. Gong, Z. Zhang, Q. Fang, Y. Zhang, J. Shi, L. Liao, X. Wu, L. Gu, Z. Liu and Y. Zhang, *Nano Lett.*, 2017, **17**, 4908–4916.
28 Z. Zhang, J. Niu, P. Yang, Y. Gong, Q. Ji, J. Shi, Q. Fang, S. Jiang, H. Li, X. Zhou, L. Gu, X. Wu and Y. Zhang, *Adv. Mater.*, 2017, **29**, 1702359.
29 H. Wang, X. Huang, J. Lin, J. Cui, Y. Chen, C. Zhu, F. Liu, Q. Zeng, J. Zhou, P. Yu, X. Wang, H. He, S. H. Tsang, W. Gao, K. Suenaga, F. Ma, C. Yang, L. Lu, T. Yu, E. H. T. Teo, G. Liu and Z. Liu, *Nat. Commun.*, 2017, **8**, 394.
30 D. Geng, X. Zhao, Z. Chen, W. Sun, W. Fu, J. Chen, W. Liu, W. Zhou and K. P. Loh, *Adv. Mater.*, 2017, **29**, 1700072.
31 B. Li, Y. He, S. Lei, S. Najmaei, Y. Gong, X. Wang, J. Zhang, L. Ma, Y. Yang and S. Hong, *Nano Lett.*, 2015, **15**, 5089–5097.

32 J. Song, G. H. Ryu, S. J. Lee, S. Sim, C. W. Lee, T. Choi, H. Jung, Y. Kim, Z. Lee, J. Myoung, C. Dussarrat, C. Lansalot-Matras, J. Park, H. Choi and H. Kim, *Nat. Commun.*, 2015, **6**, 7817.
33 Z. Lu, L. Sun, G. Xu, J. Zheng, Q. Zhang, J. Wang and L. Jiao, *ACS Nano*, 2016, **10**, 5237–5242.
34 J. Lin, Y. Lin, X. Wang, L. Xie and K. Suenaga, *APL Mater.*, 2016, **4**, 116108.
35 Z. Lin, Y. Zhao, C. Zhou, R. Zhong, X. Wang, Y. H. Tsang and Y. Chai, *Sci. Rep.*, 2015, **5**, 18596.
36 A. Gurarslan, Y. Yu, L. Su, Y. Yu, F. Suarez, S. Yao, Y. Zhu, M. Ozturk, Y. Zhang and L. Cao, *ACS Nano*, 2014, **8**, 11522–11528.
37 D. Hu, G. Xu, L. Xing, X. Yan, J. Wang, J. Zheng, Z. Lu, P. Wang, X. Pan and L. Jiao, *Angew. Chem., Int. Ed.*, 2017, **56**, 3611–3615.
38 C. H. Lee, W. McCulloch, E. W. Lee, L. Ma, S. Krishnamoorthy, J. Hwang, Y. Wu and S. Rajan, *Appl. Phys. Lett.*, 2015, **107**, 193503.
39 Y. Lee, L. Yu, H. Wang, W. Fang, X. Ling, Y. Shi, C. Lin, J. Huang, M. Chang and C. Chang, *Nano Lett.*, 2013, **13**, 1852–1857.
40 D. L. Ma, J. P. Shi, Q. Q. Ji, K. Chen, J. B. Yin, Y. W. Lin, Y. Zhang, M. X. Liu, Q. L. Feng and X. J. Song, *Nano Res.*, 2015, **8**, 3662–3672.
41 T. Liang, S. Xie, W. Fu, Y. Cai, C. Shanmugavel, H. Iwai, D. Fujita, N. Hanagata, H. Chen and M. Xu, *Nanoscale*, 2017, **9**, 6984–6990.
42 S. Lai, J. Jeon, Y. Song and S. Lee, *RSC Adv.*, 2016, **6**, 57497–57501.
43 H. R. Hoekstra, *Inorg. Nucl. Chem. Lett.*, 1973, **9**, 1291–1301.
44 E. R. Van Artsdalen and I. S. Yaffe, *J. Phys. Chem.*, 1955, **59**, 118–127.
45 U. V. Choudary, K. A. Gingerich and J. E. Kingcade, *J. Less-Common Met.*, 1975, **42**, 111–126.
46 M. Steinberg and K. Schofield, *J. Chem. Phys.*, 1991, **94**, 3901–3907.
47 Y. Liu, H. Nan, X. Wu, W. Pan, W. Wang, J. Bai, W. Zhao, L. Sun, X. Wang and Z. Ni, *ACS Nano*, 2013, **7**, 4202–4209.
48 X. Zhang, X. Qiao, W. Shi, J. Wu, D. Jiang and P. Tan, *Chem. Soc. Rev.*, 2015, **44**, 2757–2785.
49 Q. Ji, Y. Zhang, T. Gao, Y. Zhang, D. Ma, M. Liu, Y. Chen, X. Qiao, P. Tan and M. Kan, *Nano Lett.*, 2013, **13**, 3870–3877.
50 H. Zeng, J. Dai, W. Yao, D. Xiao and X. Cui, *Nat. Nanotechnol.*, 2012, **7**, 490–493.
51 X. Zhang, W. P. Han, J. B. Wu, S. Milana, Y. Lu, Q. Q. Li, A. C. Ferrari and P. H. Tan, *Phys. Rev. B: Condens. Matter Mater. Phys.*, 2013, **87**, 115413.
52 M. Buscema, G. A. Steele, H. S. J. van der Zant and A. Castellanos-Gomez, *Nano Res.*, 2014, **7**, 561–571.
53 B. Chakraborty, A. Bera, D. Muthu, S. Bhowmick, U. V. Waghmare and A. K. Sood, *Phys. Rev. B: Condens. Matter Mater. Phys.*, 2012, **85**, 161403.
54 V. Senthilkumar, L. C. Tam, Y. S. Kim, Y. Sim, M. Seong and J. I. Jang, *Nano Res.*, 2014, **7**, 1759–1768.
55 A. Splendiani, L. Sun, Y. Zhang, T. Li, J. Kim, C. Chim, G. Galli and F. Wang, *Nano Lett.*, 2010, **10**, 1271–1275.
56 K. F. Mak, K. He, C. Lee, G. H. Lee, J. Hone, T. F. Heinz and J. Shan, *Nat. Mater.*, 2013, **12**, 207–211.
57 H. Kim, D. Ovchinnikov, D. Deiana, D. Unuchek and A. Kis, *Nano Lett.*, 2017, **17**, 5056–5063.
58 K. Chen, Z. Chen, X. Wan, Z. Zheng, F. Xie, W. Chen, X. Gui, H. Chen, W. Xie and J. Xu, *Adv. Mater.*, 2017, **29**, 170704.
59 Z. Wang, Y. Xie, H. Wang, R. Wu, T. Nan, Y. Zhan, J. Sun, T. Jiang, Y. Zhao, Y. Lei, M. Yang, W. Wang, Q. Zhu, X. Ma and Y. Hao, *Nanotechnology*, 2017, **28**, 325602.
60 J. W. Matthews, *J. Vac. Sci. Technol.*, 1966, **3**, 133–145.
61 L. Shi, K. Chen, R. Du, A. Bachmatiuk, M. H. Rümmeli, M. K. Priydarshi, Y. Zhang, A. Manivannan and Z. Liu, *Small*, 2015, **11**, 6302–6308.
62 D. Lu, D. J. Baek, S. S. Hong, L. F. Kourkoutis, Y. Hikita and H. Y. Hwang, *Nat. Mater.*, 2016, **15**, 1255–1260.